Mixing Enhancement from Severely Overexpanded Nozzles

Dimitri Papamoschou[a] and Andrew D. Johnson[b]
University of California, Irvine, Irvine, CA, 92697-3975

Abstract

Flow exiting a convergent-divergent nozzle operated at severely overexpanded conditions, such that a shock wave is formed inside the nozzle, exhibits a strong instability that causes mixing enhancement in the flow itself and can destabilize an adjacent flow. The latter property enables mixing enhancement of an arbitrary jet via axial injection of a secondary gas flow. A systematic investigation of this phenomenon reveals that the instability is associated with shock-induced nozzle flow separation. In this paper we review key results that demonstrate the potential of this mixing technique and provide insight into the relevant physical processes. In addition, we establish criteria for the occurrence and location of the separation shock, and construct correlations between mixing enhancement and shock strength.

1. INTRODUCTION

A strange occurrence of mixing enhancement was observed while investigating jet noise from coannular convergent-divergent (CD) nozzles. In these experiments, the jets were composed of a supersonic stream (primary flow) surrounded by a stream of variable velocity and density (secondary flow or coflow). With the conditions of the supersonic primary stream fixed and the velocity of the secondary stream increasing from subsonic to sonic to supersonic, the following trends were observed. First, the spreading rate of the primary jet decreased, as expected from the reduced velocity difference across the shear layer dividing the inner and outer streams. As the secondary stream approached sonic conditions (corresponding to ideally-expanded Mach numbers in the approximate range of 0.8 to 1.2), the spreading rate was significantly enhanced, an unexpected deviation. An example of this deviation is shown in Figure 1, where an annular coflow destabilizes a supersonic jet surrounded by the coflow. With increasing, supersonic velocity of the secondary flow, the spreading rate decreased from the enhanced state and eventually returned to normal values. The puzzling departure near the sonic point triggered a systematic investigation of this phenomenon experimentally[1-4] and computationally.[5,6] The goal of this paper is to distill results of past studies towards a cohesive understanding of this phenomenon, and present new results that provide guidance toward its practical use. Before proceeding it is useful to review the significance of mixing enhancement and the state of the art in mixing enhancement methods.

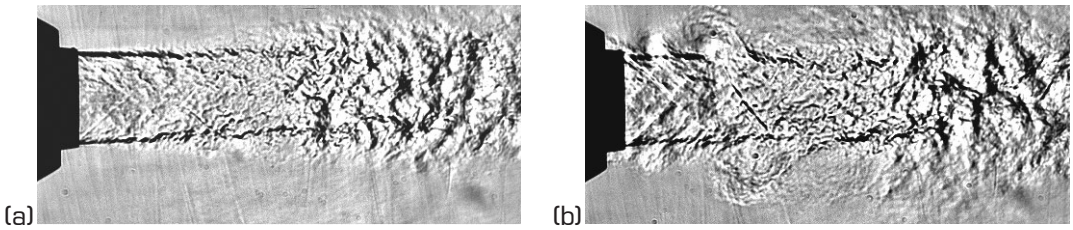

Figure 1. Effect of an unstable coflow on a Mach 1.5 jet. (a) Single jet; (b) coaxial jet.

The vast majority of our energy and propulsive power comes from burning fuels. Fuel efficiency and reduction of toxic emissions are governed by the completeness of the mixing process between fuel and oxidizer.[7] Ideally, fuel and oxidizer mix at the molecular level in the desired proportion before reacting.

[a]Professor, Department of Mechanical and Aerospace Engineering, 4200 Engineering Gateway, Irvine, CA, 92697-3975.

[b]Post Doctorate Researcher, Department of Mechanical and Aerospace Engineering, 4200 Engineering Gateway, Irvine, CA, 92697-3975.

Incomplete or non-uniform mixing leads to unburned reactants with resulting loss in efficiency and production of pollutants such as soot particles and nitric oxides.[8] The ideal case is extremely difficult to achieve in practice. A major constraint is the finiteness of space and/or time available for mixing. In the combustor of a jet engine, for instance, fuel and air must mix at high velocity within a very short length. In reciprocating engines, fuel must be introduced and mixed in the piston cylinder within a few milliseconds. These challenges apply to both gaseous and liquid fuels, although liquid fuels are more difficult to mix because a liquid stream must go through several stages before complete reaction can occur: breakup, atomization, vaporization, and molecular mixing with the oxidizer.[9] Another difficulty is the simultaneous achievement of mixing enhancement and sufficient penetration into the combustion zone. Examples where penetration is critical are injection into the cylinder of a diesel engine and transverse injection into a crossflow.[10] Conventional devices such as lobe mixers,[11] swirlers[12] and airblast atomizers[13] achieve mixing with an attendant reduction in the axial momentum of the flow, which reduces penetration. A further consideration is simplicity and compactness of the nozzles. Good mixing does not guarantee operational success if the mixer is too complicated, too large, or too heavy.

In aircraft exhaust systems, mixing enhancement has been motivated by the need to suppress noise and thermal emissions. Mechanical schemes have included lobe mixers;[14,15] vortex generators, mainly in the form of tabs;[16,17] and nozzle cutouts.[18] Major drawbacks are thrust penalty (with notable exception of the cutouts, which inflict minimal thrust loss but require imperfect expansion of the jet), weight penalty, and complexity of the engine exhaust. Thrust losses escalate with increasing jet Mach number and can easily reach the order of 10% in supersonic jets.[19-21] Complexity of the engine exhaust means increased manufacturing and maintenance costs. In the general area of high-speed shear layers, efforts to increase mixing have included cavity actuators,[22] shock impingement,[23] trailing edge modifications,[24] and sub-boundary layer disturbances.[25] The obvious tradeoff is mixing versus total pressure loss. The least-intrusive methods increase the growth rate modestly, while the forceful ones increase mixing at the expense of aerodynamic performance. Efficient mixing enhancement at high speeds remains one of the toughest challenges of fluid mechanics. For military low-observable aircraft, minimizing radar cross-section is an additional concern. Complex mechanical mixers are likely to increase the radar cross section.

The desire to find alternatives to mechanical mixers has sparked research on fluidic control of jets. The counter-current shear layer of Strykowksi et al.[26] demonstrated a substantial increase in the mixing rate compared to the classical flow. Application of a counterflow on an engine exhaust or fuel injector has the obvious drawback of momentum loss, although other properties of counter-flow have been ingeniously exploited towards thrust vectoring.[27] Significant effort has also been directed to pulsed-jet control, where unsteady transverse jets installed at the jet exit destabilize the plume.[28,29] While impressive increases in the jet entrainment rate have been recorded, practical implementation presents several challenges, including impact on system performance and loss of axial momentum. Synthetic jets are showing substantial promise in controlling subsonic gas flows; their efficacy in supersonic environments has not yet been demonstrated.[30]

The mixing enhancement method presented here differs from the aforementioned techniques in two distinct areas: first, it is a passive technique that does not employ complex mechanical devices to directly disturb the flow; second, it utilizes parallel flow to excite instability, in contrast to counter-flow and transverse-flow methods. The generic nozzle configuration is illustrated in Figure 2. Critical parameter are the ratio of exit area to throat (minimum) area, A_e/A_t, of the coflow nozzle, and the nozzle pressure ratio (NPR=p_0/p_a) supplying the coflow nozzle. The properties of the primary stream are irrelevant to the instability mechanism.

2. EXPERIMENTAL EFFORT

Our effort on this phenomenon has spanned several years and hundreds of experiments in various facilities. Related computational and experimental efforts have also been conducted at other institutions.[2,5,6] Here we review key experiments conducted at U.C. Irvine that demonstrate the overall capabilities of this mixing enhancement method and explain some of the salient physics. We begin with a brief description of the facilities involved, followed by a presentation of the results. Since we discuss both internal and external flows, we introduce two axial coordinate systems. Lower-case x is used for the internal flows and its origin is at the nozzle throat. Upper-case X is used for the flow outside the nozzle, and its origin is at the nozzle exit plane. Normalizations involve the jet diameter D or the nozzle throat height H_t.

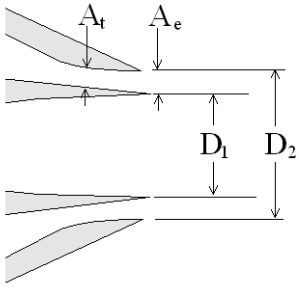

Figure 2 Generic shape of mixing-enhancement nozzle. Outer (coflow) duct is convergent-divergent.

2.1 Facilities and Diagnostics

A large number of experiments were conducted in the small-scale coaxial jet facility depicted in Figure 3. The inner nozzles of 12.7 mm exit diameter were designed by the method of characteristics for Mach numbers M_1=1.5, 1.75, and 2.00. This paper discusses the Mach 1.5 tests. A variety of outer nozzles formed the annular passage for the coflow. Precisely metered mixtures of helium and air were supplied to the nozzles, which exhausted into the ambient, still air. Helium-air mixtures effectively duplicate well the density, velocity, and speed of sound of a heated jet.

The experiments in the round facility indicated that the source of the mixing enhancement is related to the convergent-divergent secondary nozzle. It thus became imperative to build a larger facility dedicated to the study of flow and wave phenomena in CD nozzles. The resulting apparatus is depicted in Figure4. It features a planar nozzle formed between two flexible aluminum plates. The plates can be bent using two set of actuators to alter the exit-to-throat area ratio (A_e/A_t), nozzle contour, and maximum wall angle. Asymmetric nozzles, or half nozzles, can be obtained by deflecting only one plate. The sidewalls of the nozzle are composed of precision ground optical windows to allow full visual access to the internal flowfield. The nominal test section dimensions are 17.8 mm in height, 63.5 mm in width, and 117 mm in length from throat to exit, resulting in a nozzle aspect ratio of AR=3.57. In this investigation the range of nozzle pressure ratios studied was NPR=1.2-1.8, generally resulting in the formation of an internal shock. This corresponds to Reynolds numbers, based on the throat height, of Re=2.23×10^5-4.81×10^5 and perfectly expanded Mach numbers of M_{pe}=0.52-0.96.

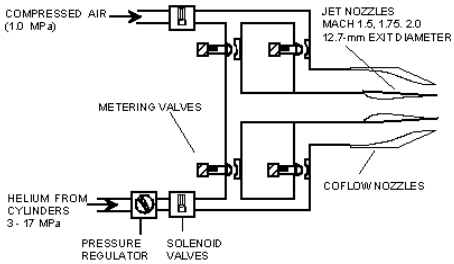

Figure 3 Coaxial jet facility.

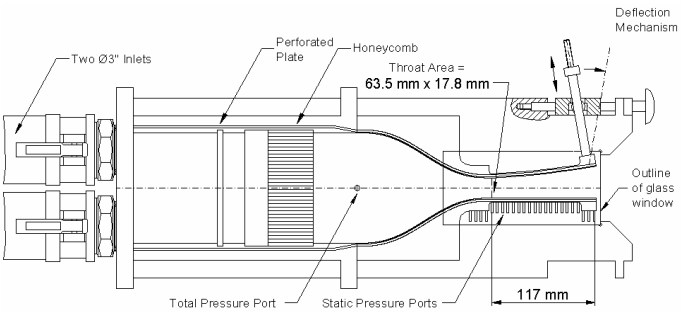

Figure 4 Schematic of apparatus for the study of supersonic nozzle flow separation and shock unsteadiness.

For both facilities, flow visualization was achieved using a schlieren photography system with a 20 nanosecond spark source (Xenon, Model N787). This system was arranged on a mobile support table that could be coupled with either nozzle facility. The optics layout included two 150 mm lenses with a focal length of 1 m used to collimate the beam of light through the test section. A portion of the emerging light beam was intercepted using an adjustable pinhole placed at the focal point. Images were obtained using a CCD camera with a spatial resolution of 576×384 pixels.

Plume surveys utilized a Pitot rake system attached to a three-dimensional motorized traverse. The rake consisted of five 1-mm internal diameter probes, each 70 mm long, spaced 10 mm apart on a streamlined mounting plate. Each Pitot probe was individually connected to a capacitance-type pressure transducer. Additionally, the planar nozzle facility was equipped with static ports on the upper and lower test section walls, as well as piezoelectric pressure transducers that measured the instantaneous wall pressure distribution in a localized area of the nozzle.

2.2 Experiments in axisymmetric nozzles

Figure 5 presents schlieren images of three jet flows, all involving the same primary air jets at Mach 1.5: Figure 5a depicts the single jet; Figure 5b depicts the jet surrounded by a coflow from a convergent nozzle; and Figure 5c depicts the jet surrounded by a convergent-divergent nozzle. In the dual stream cases, the coflow was supplied at a nozzle pressure ratio of NPR=1.75 and the mass flow rates were equal. Introduction of the coflow from the convergent nozzle, Figure5b, reduced the velocity difference across the jet's shear layer, thereby stabilizing the jet. If instead the coflow is supplied by the convergent-divergent nozzle, Figure 5c, instability is introduced into the emerging jet.

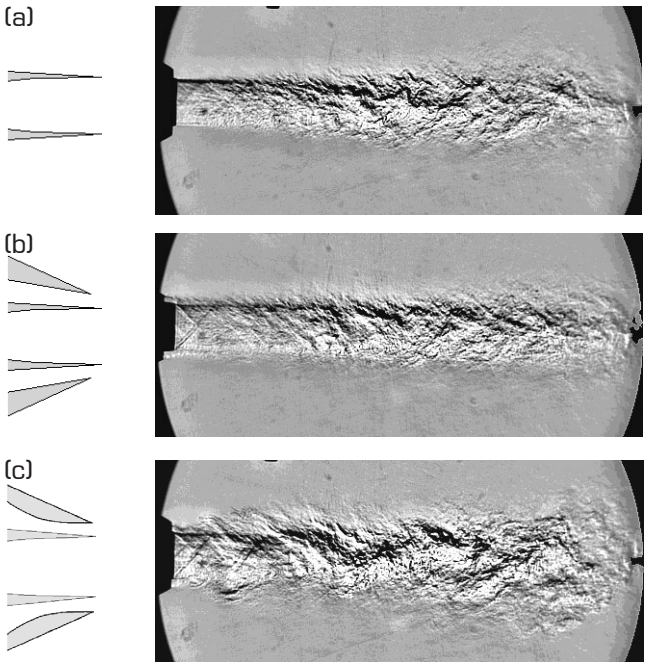

Figure 5 Schlieren images of Mach 1.5, 450 m/s air jets: (a) no coflow; (b) coflow issuing from a convergent annular duct; (c) coflow issuing from a convergent-divergent annular duct with A_e/A_t=1.25.

A quantitative measure of mixing enhancement in jets is the decay of the centerline Mach number with axial distance. Faster decay implies stronger mixing between the primary flow and ambient fluid. Figure 6 shows the centerline Mach number distributions for the three cases present in Figure 5. The potential core of the single jet ends at rough X/D_1=6.0. Introducing a coflow stream from a convergent nozzle results in the elongation of the potential core to X/D_1=8.0, while introducing a coflow from a convergent-divergent nozzle shortens the potential core to X/D_1=4.0. A proper quantitative assessment of mixing enhancement should compare two cases of equal mass flow rate and equal thrust. This is possible here by comparing the axial Mach number distributions of the two coaxial flows, which have equal mass flow rate and roughly (within a few percent) equal thrust. The divergence of the coflow

nozzle resulted in a 50% reduction in the length of the potential core and a 40% reduction in the axial Mach number at x/D_1=10.0. The unequal comparison between the single jet of Figure 5a and the combined flow of Figure 5c (which has 42% more mass flow rate and 29% higher thrust than the single jet) shows that the coaxial flow mixed faster with the surrounding air than did the single jet. In other words, addition of the coflow resulted here in net mixing enhancement. Obviously if the coflow became very large, this would not be the case. Net mixing enhancement between the inner jet and the ambient fluid is expected to occur if the mass flow rate of the coflow is a fraction of that of the jet. Figure 7 presents the variation of centerline Mach number at X/D_1=10 versus coflow nozzle pressure ratio for the arrangement of Figure 5c. As NPR increased from 1.0, the centerline Mach number increased, signifying mixing suppression. At around NPR=1.4, the trend reversed and the centerline Mach number declined rapidly (mixing enhancement), staying at low levels until about NPR=2.5. Above this NPR, the centerline Mach number rose to values that seem consistent with the lack of mixing enhancement.

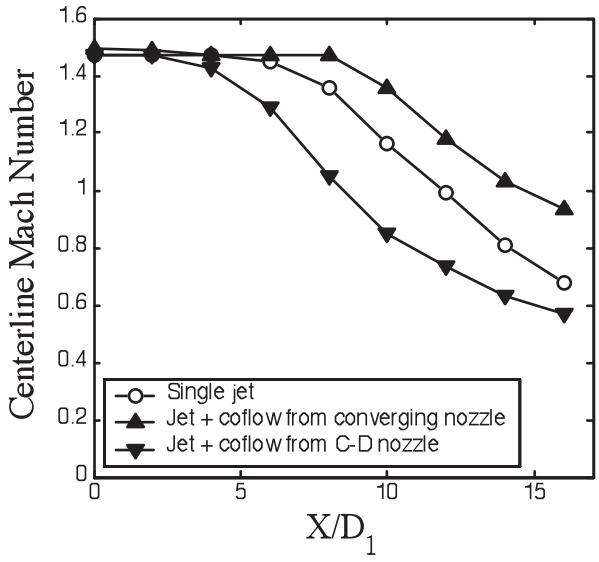

Figure 6 Centerline Mach number distributions for cases of Figure 5.

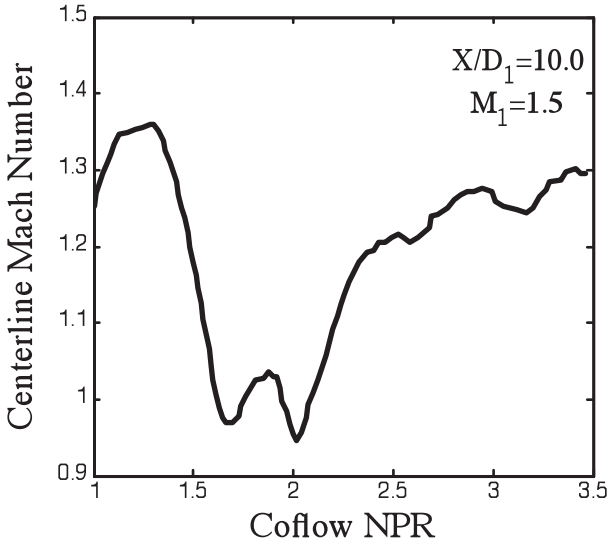

Figure 7 Centerline Mach number at x/D_1=10 versus coflow NPR for the arrangement of Figure 5c. Inner flow is a Mach 1.5 air jet.

We will now consider cases of single stream annular nozzles, where the inner nozzle has been replace by a streamline plug. In this case, the coflow nozzle alone is responsible for the emerging jet. Figure 8 compares schlieren images of two such jets, one exhausting from an annular convergent nozzle and the other from an annular convergent-divergent nozzle with an exit-to-throat area ratio of A_e/A_t=1.25. Both nozzles were supplied by a helium-air mixture at a nozzle pressure ratio of NPR=1.75 and produced the same mass flow rate. The jet from the convergent-divergent nozzle spread roughly three times faster than the jet from the convergent nozzle. Figure 9 shows the axial variation of centerline Mach number $M_{C/L}$ for the cases similar to those of Figure 8 but with air replacing the helium-air mixture. The instability associated with the convergent-divergent nozzle caused a substantial decrease in $M_{C/L}$ starting at a short distance from the nozzle exit. The reduction reached 40% at X/D_2=5. Figure 10 shows the variation of $M_{C/L}$ with NPR at a fixed axial position of X/D_2=5.7 for the two configurations of Figure 8, with air in the coflow. As NPR increased from 1.0, $M_{C/L}$ rose identically for both nozzles until NPR=1.36 was reached. Immediately past this value, $M_{C/L}$ for the convergent-divergent nozzle dropped with increasing NPR, while $M_{C/L}$ for the convergent nozzle

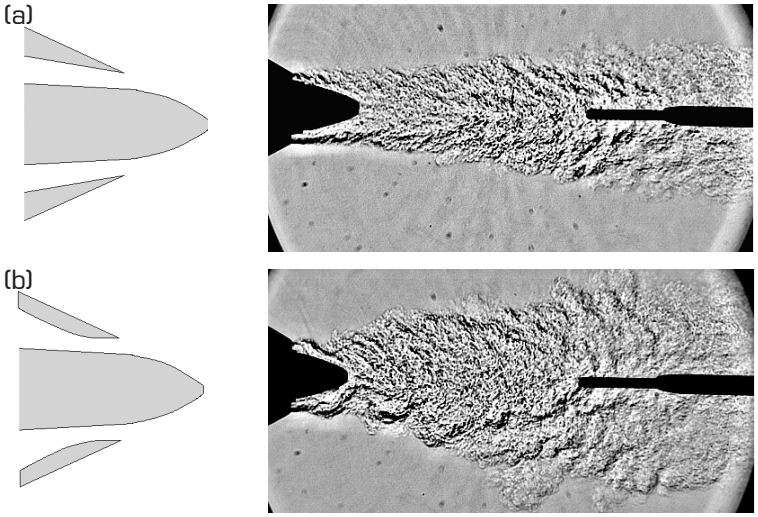

Figure 8. Schlieren images of annular jets composed of a helium-air mixture. Ideally expanded Mach number is 0.9 and velocity is 410 m/s for both jets. (a) Annular nozzle is convergent; (b) annular nozzle is convergent-divergent with A_e/A_t=1.25.

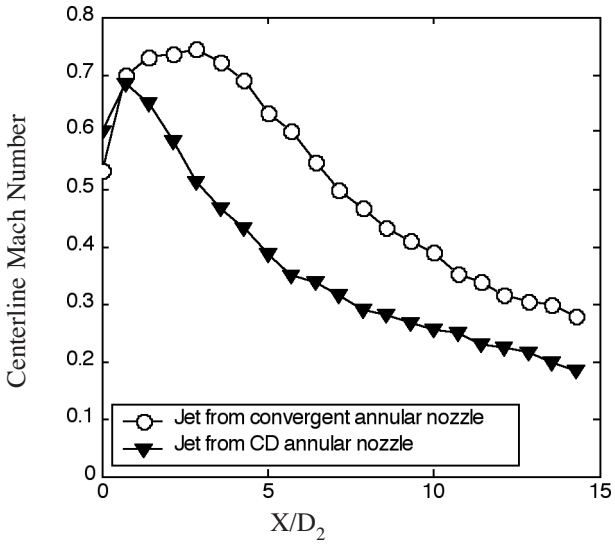

Figure 9 Centerline Mach number distributions for annular air jest issuing from a convergent nozzle and from a convergent-divergent nozzle. NPR=1.68 and the mass flow rate was equal for both jets.

continued rising. Thus, NPR=1.36 marks the start of the mixing enhancement for this particular nozzles. At NPR≈1.5, the $M_{C/L}$ for the convergent-divergent nozzle started rising again but at a value about 40% below that of the convergent nozzle. The difference between the two nozzles closed at around NPR=3.0, which suggests the end of mixing enhancement. The best mixing enhancement, in terms of percent drop in $M_{C/L}$, occurred for 1.5<NPR<2.5.

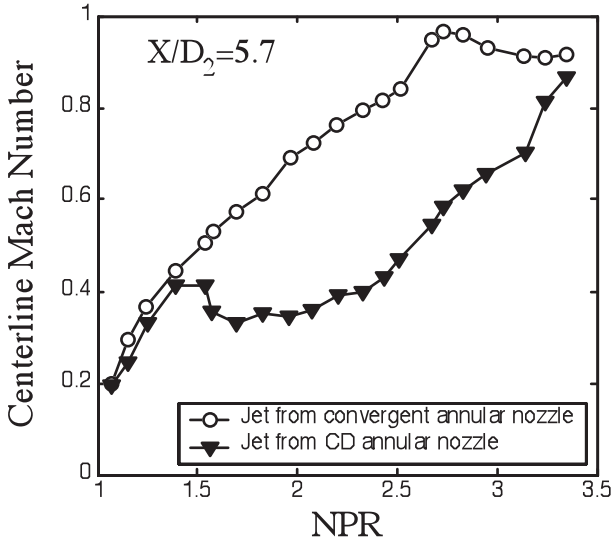

Figure 10 Centerline Mach number at X/D_2=5.7 versus NPR for annular air jets issuing from a convergent nozzle and from a convergent-divergent nozzle. At each NPR, the two jets had the same mass flow rate.

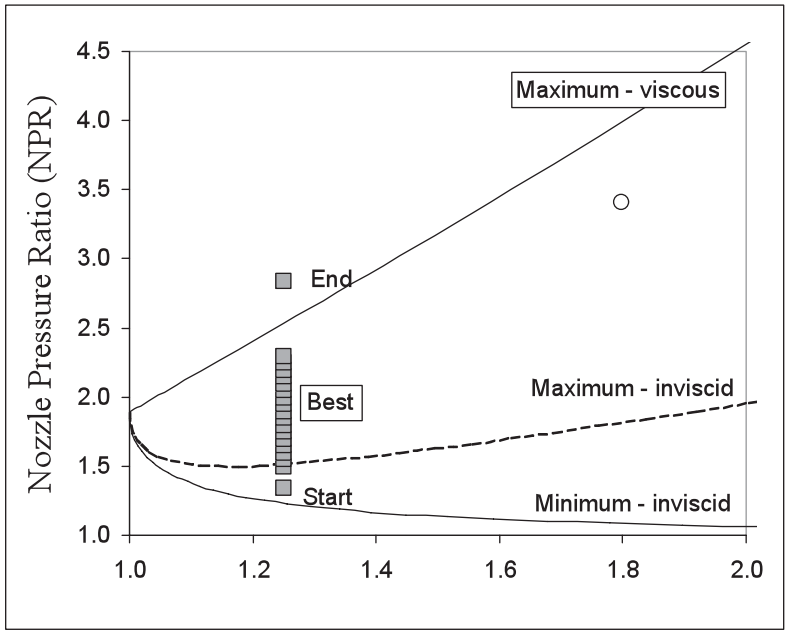

Figure 11. Prediction of NPR versus nozzle area ratio for shock-containing nozzle flow. The theoretical lower limit is based on inviscid, 1D calculation for the onset of sonic flow. The inviscid upper limit is based on 1D flow, while the viscous upper limit is based on the normal-shock separation solution of Romine (Ref. 31) and is more realistic. Rectangular symbols depict experiment data on the onset, strongest occurrence, and cessation of mixing enhancement in an axisymmetric nozzle with A_e/A_t=1.25. The round symbol denotes the pressure ratio for which a normal shock is visualized at the exit of nozzle with area ratio 1.8 (Ref.36).

Figure 11 presents an important summary of the above results. The onset, best performance, and cessation of mixing enhancement is plotted on the NPR-A_e/A_t diagram for the cases with A_e/A_t =1.25. The solid lines represent the minimum and maximum NPR for formation of a shock inside the nozzle. The relations for shock formation will be discussed in Section 3.1. The critical observation is that mixing enhancement is associated with shock formation inside the nozzle, i.e., the phenomenon of supersonic nozzle flow separation. This motivated the fundamental study of flow inside and outside a convergent-divergent nozzle, outlined in the next section.

2.3 Experiments in planar nozzles

The planar nozzle facility enabled a fundamental study of shock and flow phenomena associated with supersonic nozzle flow separation. Here we review results that illuminate the flow structure, separation conditions, and plume development.

2.3.1 Flow Structure

In the one-dimensional, inviscid-wall treatment of shock-containing nozzle flow, the shock structure is perfectly normal with the flow remaining attached to the walls downstream, resulting in a subsonic compression to the ambient static pressure. In the actual, viscous case, the shock acquires a bifurcated structure and the adverse pressure gradient across the shock feet causes the flow to detach from the sidewalls of the nozzle forming separation regions downstream. Figure 12a shows a typical schlieren image of a shock formation inside the planar nozzle facility and Figure 12b is a schematic of the flowfield. Near the wall, the separation shock consists of incident and reflected oblique waves that merge into a Mach stem at the triple point. This is the so-called lambda foot of the shock. The adverse pressure gradient through the shock forces the incoming boundary layer to separate, forming separation regions downstream. The oblique shock structures are of the "weak" type resulting in low supersonic flow downstream while the flow immediately past the Mach stem is subsonic. The trailing shocks reflect from the separation shear layers as expansion fans that propagate across the test section to the

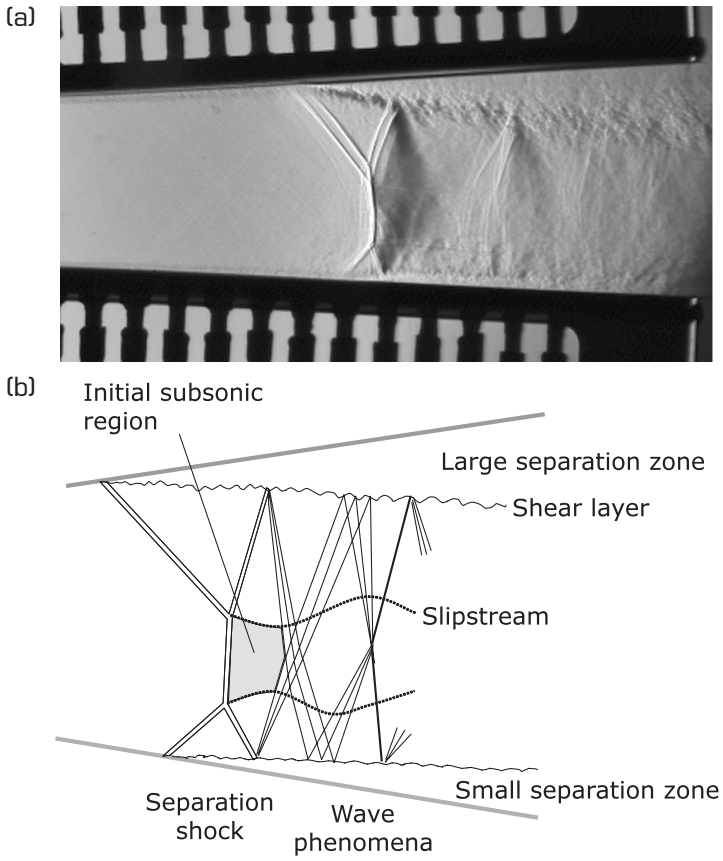

Figure12 Shock-induced nozzle flow separation. (a) Spark schlieren image; (b) schematic of principal flow and wave phenomena.

opposite shear layers where they are reflected again as compression waves. Slipstreams emerging from the triple points form a convergent-divergent channel which, in concert with the expansion fans, accelerates the subsonic flow downstream of the normal portion of the shock to supersonic speed. Except at low pressure ratios and area ratios, the shock structure is asymmetric, as shown in Figure 12, with one lambda foot-separation pair larger than the other. Several analytical models[31,32] as well as numerical investigations[5,33-35] have shown agreement on this basic structure of the shock separation. The asymmetry is an important aspect of the mixing enhancement mechanism as it provides room for the large separation shear layer to become very unstable and grow to large size inside and outside the nozzle.[4]

The departure of the real flow from the one-dimensional model has a profound effect on the shock location. Figure 13 compares shock locations, obtained from instantaneous visualizations, with the one-dimensional prediction for a nozzle with A_e/A_t=1.4. The structure of the actual flow creates a back pressire p_b for the shock back pressure that is much higher than that predicted by one-dimensional theory. As a result, for a given NPR, the shock sits much closer to the throat than predicted.

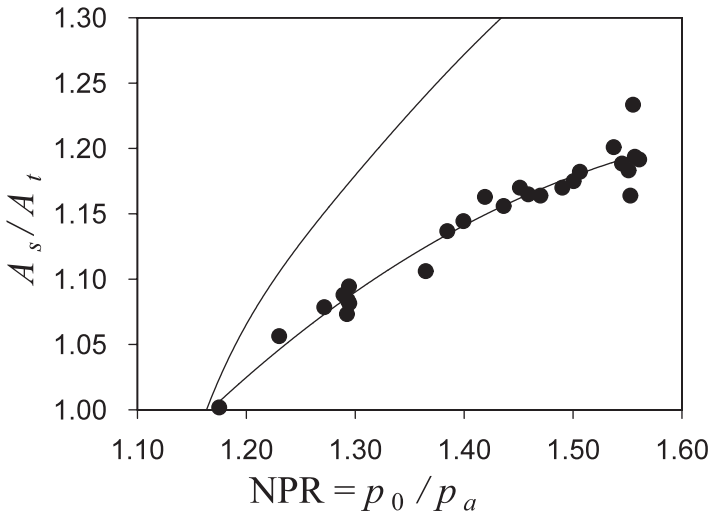

Figure 13 Shock location versus NPR for a planar nozzle with A_e/A_t=1.40. Thin line is best fit of data, thick line is prediction of inviscid, 1D theory.

2.3.2 Wall Pressure Distributions

We examine the time-averaged wall pressure distributions with an eye toward developing a prediction method for flow separation. For this reason, instead of the traditional normalization of p/p_0, we plot instead p/p_a. Shown in Figure14 are axial distributions of p/p_a at different NPRs for nozzles with A_e/A_t =1.2, 1.3, 1.4, and 1.5. For each distribution, the shock formation and gradual recovery to ambient pressure is evident. The separation pressure p_s is defined as the lowest pressure before the shock jump.

The separation pressure p_s/p_a shows a remarkable consistence for all the cases plotted in Figure 14. It ranges from p_s/p_a =0.55 at A_e/A_t=1.2 to p_s/p_a=0.47 at A_e/A_t =1.5. These numbers are consistent with the findings of Hunter[36] in planar nozzles. Importantly, for a given nozzle area ratio, the separation pressure does not vary appreciably with NPR. This suggests that p_s/p_a is not a function of the shock Mach number M_s, as suggested by Hunter,[36] but rather a function (albeit a weak one) of nozzle area ratio. For the range of area ratios and pressure ratios relevant to the mixing enhancement phenomenon, a "rule of thumb" p_s/p_a=0.5 gives a satisfactory prediction of the separation pressure and hence of the shock location.

2.3.3 Plume Surveys

Mean velocity surveys of the jet plume emerging from the planar nozzle were performed using the Pitot rake system. The surveys comprised 2D scans along the transverse centerplane of the nozzle as well as a limited amount of 3D scans. The 3D scans revealed that mixing enhancement occurs primarily in the transverse direction, thus the 2D scans provide adequate information to characterize the growth of the plume.

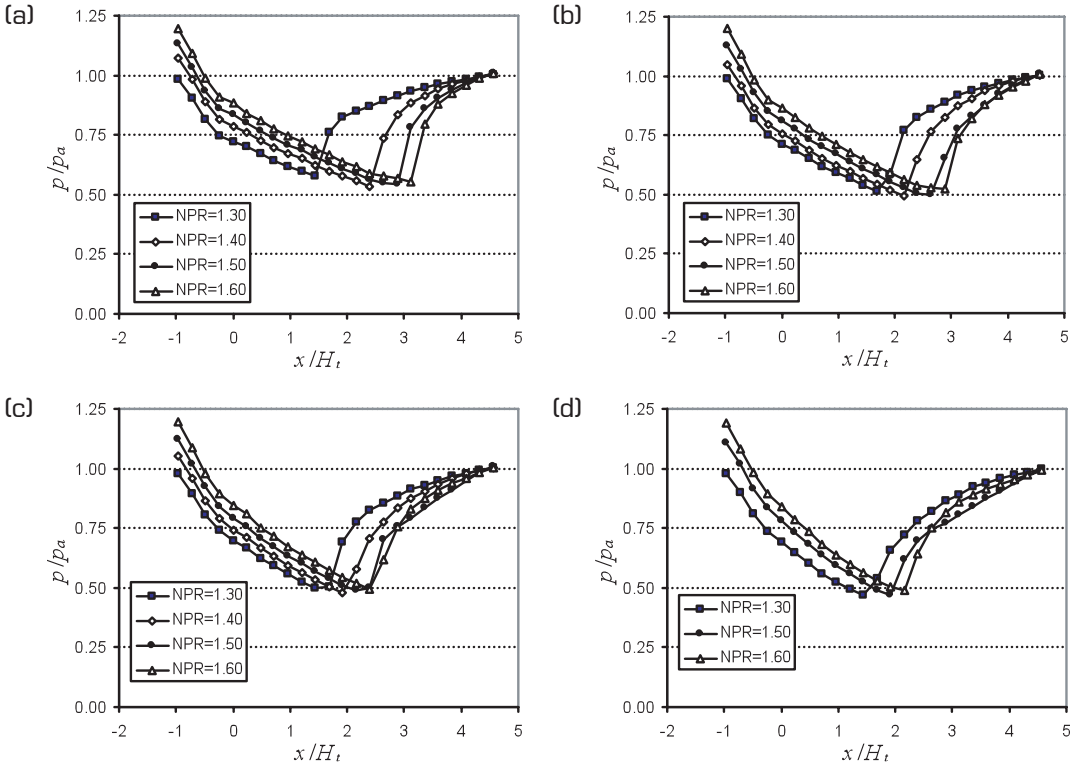

Figure 14. Wall pressure distributions for various nozzle pressure ratios. (a) A_e/A_t=1.2; (b) A_e/A_t=1.3; (c) A_e/A_t=1.4; (d) A_e/A_t=1.5.

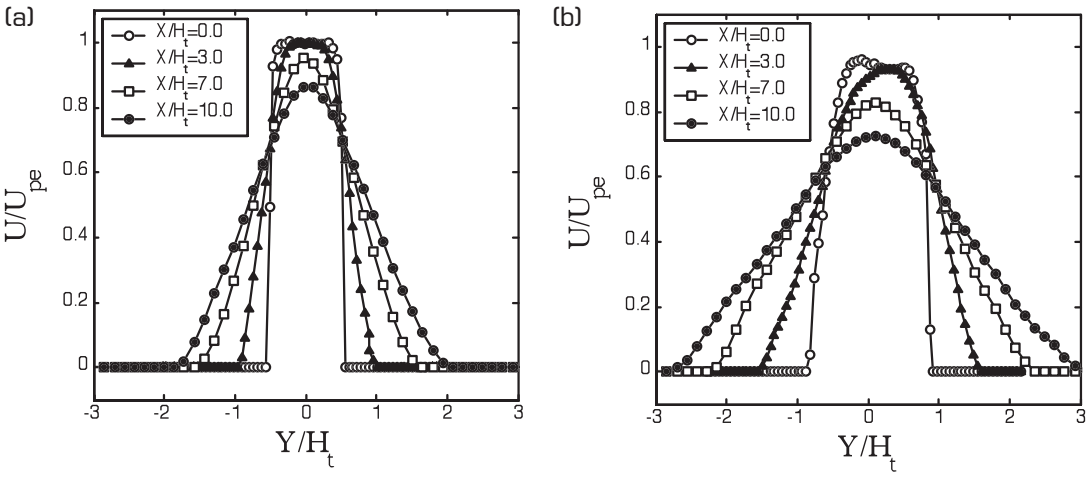

Figure 15 Transverse velocity profiles at various axial locations for NPR=1.6 and: (a) A_e/A_t=1.0; (b) A_e/A_t=1.6.

Figure 15 compares the axial development of mean velocity for a baseline configuration of A_e/A_t=1.0 and an overexpanded shock-containing case of A_e/A_t=1.6 for the same nozzle pressure ratio NPR=1.6. The exit profile (X/H_t=0) for the baseline case is symmetric and has a "top hat" shape, shown in Figure 15a. The peak velocity here is equal to the perfectly expanded velocity, signifying negligible total pressure loss through the nozzle. Progressing downstream from the nozzle exit, the jet spreads symmetrically and the peak velocity decreases. The exit profile for the shock-containing case, shown in Figure 15b, is significantly different than that of the baseline case. The profile is asymmetric and has a double lobed shape due to the asymmetric internal shock/separation structure, shown in Figure 11. The flow passing through the normal (Mach stem) portion of the shock wave experiences a greater

total pressure loss than the flow passing through the oblique lambda feet, resulting in a local minimum in velocity near the centerline of the emerging jet. The smoother edges in the exit profile result from the presence of the developed separation shear layers. In this case, the jet spreads asymmetrically downstream at a rate at which is noticeably higher than the baseline case, signifying stronger mixing.

Figure 16 shows the peak velocity distributions versus axial distance for a nozzle pressure ratio of NPR=1.6 and increasing nozzle area ratio A_e/A_t=1.0-1.8. There are pronounced increases in the rate of decay of peak velocity with increasing nozzle area ratio. This correlates to nearly a 50% reduction in the length of the potential core between exit-to-throat area ratio A_e/A_t=1.0 and A_e/A_t=1.8, accompanied by a 20% reduction in peak velocity at the axial position of X/H_t=10.0. These results suggest that for a fixed nozzle pressure ratio, mixing enhancement is achieved by increasing nozzle area ratio.

The jet thickness at a given axial position is defined here as the transverse distance spanning the region of the velocity profile where the mean velocity exceeds 20% of the maximum value. Figure 17 plots jet thickness distribution with axial distance for a nozzle pressure ratio of NPR=1.6 and increasing nozzle area ratio A_e/A_t=1.0-1.8. It should first be noted that the exit thickness of the jet, δ_e, increases with increasing nozzle area ratio such that its value is approximately equal to the exit height of the

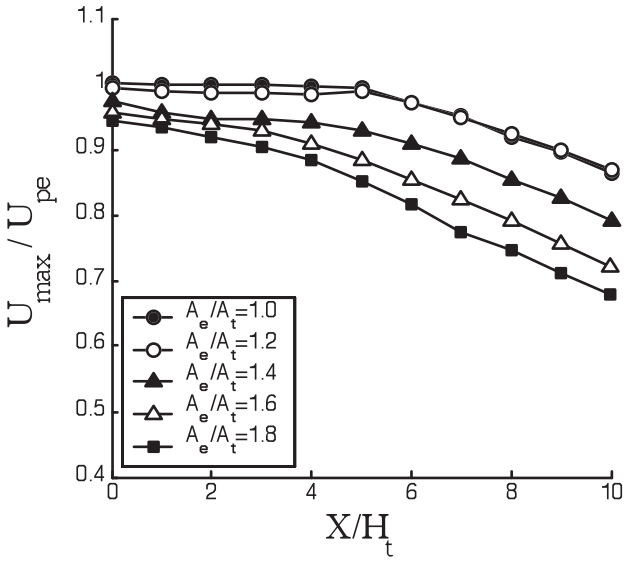

Figure 16 Peak Velocity decay for NPR=1.6 and increasing exit-to-throat nozzle area ratio.

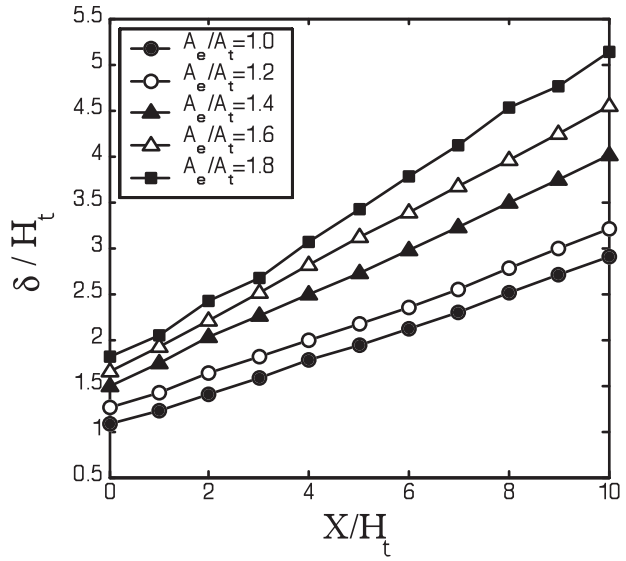

Figure 17 Jet thickness distribution for NPR=1.6 and increasing exit-to-throat nozzle area ratio.

nozzle, H_e. This indicates significant spreading of the internal separation jet prior to exiting the nozzle. Downstream of the nozzle exit, the jet thickness grows linearly and at a rate that is amplified with increasing nozzle area ratio, evident by the increase in slope.

2.3.4 Shock Unsteadiness

Johnson and Papamoschou[4] conducted a series of time-resolved experiments involving simultaneous tracking of the shock motion and total pressure measurement in the downstream flow. The shock position was monitored with an array of wall pressure transducers, and the total pressure was measured with a dynamic Pitot probe. There are two key findings of these experiments that help explain the mixing enhancement phenomenon. First, as the strength of the shock (quantified in terms of the shock Mach number M_s) is increased, the shock becomes more unstable. The shock motion histories in Figure 18 demonstrate this effect clearly, where x_s' is the shock position fluctuation about its mean location. The range of the motion increases significantly as M_s rises from 1.48 (Figure 18a) to 1.67 (Figure 18b). Second, this large-scale motion of the shock excites instability in the downstream flow, evident by significant correlation between the shock motion and total pressure fluctuation far downstream. Because the separation shear layer originates at the shock foot (Figure12), the motion of the shock amounts to a forcing of the separation shear layer. The shear layer appears most susceptible to large-amplitude, low-frequency disturbances which become more prevalent with increasing shock strength. The asymmetry of the separation contributes to the shear layer instability by allowing the large shear layer substantial room to grow. In terms of mixing enhancement, these results imply that stronger shocks should produce better mixing, a hypothesis that we test in the next section.

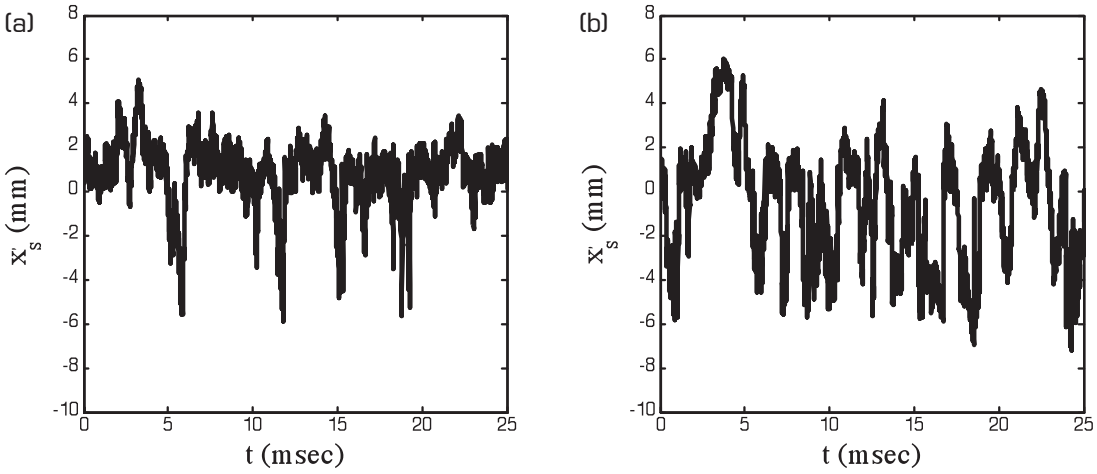

Figure 18 Shock-position fluctuation trace for a shock Mach number (a) M_s=1.48 and (b) M_s=1.67.

3. ANALYSIS

It is evident from the preceding results that shock formation inside the nozzle is a necessary condition for the occurrence of the mixing enhancement phenomenon. Several issues arise that are critical both for fundamental understanding and for prediction of mixing enhancement. First, we would like to be able to predict the conditions under which the shock is located inside the nozzle; second, we need a tool to predict the shock location (strength) versus nozzle pressure ratio and area ratio; and third, we seek a correlation of mixing enhancement versus shock strength.

3.1 Shock Location

The range of nozzle pressure ratios where a shock wave is present in the nozzle is dependent on the nozzle area ratio. The minimum NPR corresponds to the condition where sonic flow develops at the throat of the nozzle. To find this NPR we first solve for the exit Mach number using the subsonic branch of the Mach area relation

$$\left(\frac{A_e}{A_t}\right)^2 = \left(\frac{1}{M_e^2}\right)\left[\frac{2}{\gamma+1}\left(1+\frac{\gamma-1}{2}M_e^2\right)\right]^{\frac{\gamma+1}{\gamma-1}} \tag{1}$$

and calculate the NPR from the total-to-static pressure relation

$$NPR_{\min} = \frac{p_0}{p_a} = \frac{p_0}{p_e} = \left(1+\frac{\gamma-1}{2}M_e^2\right)^{\frac{\gamma}{\gamma-1}} \tag{2}$$

As the nozzle pressure ratio is increased, the shock wave will eventually be pushed to the exit of the nozzle, resulting in shock-free internal flow. Denoting s and b the conditions immediately fore and aft of the shock, the one-dimensional, inviscid prediction for this condition is

$$NPR_{\max} = \frac{p_0}{p_a} = \frac{p_0}{p_b} = \frac{p_0/p_s}{p_b/p_s} = \frac{\left(1+\frac{\gamma-1}{2}M_s^2\right)^{\frac{\gamma}{\gamma-1}}}{1+\frac{2\gamma}{\gamma+1}\left(M_s^2-1\right)} \quad \text{(inviscid)} \tag{3}$$

where the numerator is the total-to-static pressure ratio immediately ahead of the shock and the denominator is the static pressure ratio across the shock. The shock Mach number M_s is given by the supersonic branch of Eq. 1. However, as we saw in Figure 13, the one-dimensional theory grossly underestimates the NPR required to position the shock at a given area ratio. Therefore, we need a more realistic prediction of the NPR for which the shock sits at the exit.

There is a large volume of literature dealing with separation in rocket nozzles, which have large expansion ratios. A paramount issue is prediction of separation location, specifically the ratio p_s/p_a (pressure just ahead of separation over ambient pressure). An extensive review of the older literature, and correlation of experimental results in a large variety of nozzles, is given by Morrisette and Goldberg.[37] Their primary conclusion is that zero-pressure-gradient separation predictors, like the method of Reshotko and Tucker,[38] give reasonable predictions for nozzles with turbulent separation and large divergence angles. The ratio p_s/p_a is a declining function of the shock Mach number M_s and, as a rule of thumb, is roughly 0.5 for $M_s \approx 2$ and 0.3 $M_s \approx 4$. Even though these correlations derive from nozzles with large area ratios, they are consistent with the criterion $p_s/p_a \approx 0.5$ found for nozzles with moderate expansion ratios in our study, as well as the study by Hunter.[36] However this criterion is not expected to hold as $A_e/A_t \to 1$ or when the shock is located at the nozzle exit.

To develop a more robust criterion for the NPR at which the shock sits at the nozzle exit, we turn to Romine's model of nozzle flow separation.[32] For shocks with moderate Mach numbers ($M_s \leq 2.25$), as is the case here, Romine postulates that the jet flow emerging from the shock is above ambient pressure and adjusts to the ambient pressure via a gradual underexpansion. The magnitude of the underexpansion is equal to that of the overexpansion, i.e., $p_b/p_a = p_a/p_s$. Accordingly $p_a/p_s = (p_b/p_s)^{1/2}$, and the relation for predicting the nozzle pressure ratio at which the shock is pushed to the nozzle exit becomes

$$NPR_{\max} = \frac{p_0}{p_a} = \frac{p_0/p_s}{\sqrt{p_b/p_s}} = \frac{\left(1+\frac{\gamma-1}{2}M_s^2\right)^{\frac{\gamma}{\gamma-1}}}{\sqrt{1+\frac{2\gamma}{\gamma+1}\left(M_s^2-1\right)}} \quad \text{(viscous)} \tag{4}$$

Returning to Figure 11, we now explain the line plots that describe shock formation inside the nozzle. The "minimum-inviscid" plot refers to the minimum NPR obtained by Eqs. 1 and 2; it is a reasonable approximation for the onset of shock formation inside the nozzle. The "maximum-inviscid" curve refers to the maximum NPR for shock inside the nozzle as predicted by one-dimensional, inviscid-wall theory (Eq. 3). Finally, the "maximum-viscous" curve refers to the more realistic maximum NPR inferred by Romine's model, Eq.4. Included in the plot is an experimental datum by

Hunter[36] for positioning the shock at the exit of a nozzle A_e/A_t=1.8.

In summary, Equations 1, 2, and 4 provide the range of pressure ratios for which a shock is expected to form inside a nozzle with a given area ratio A_e/A_t. Once the shock is inside the nozzle (and sufficiently upstream of the exit), its location and strength can be determined by the separation criterion $p_s/p_a \approx 0.5$. Specifically, the shock Mach number is given by the relation

$$M_s = \sqrt{\frac{2}{\gamma - 1}\left[\left(\frac{NPR}{p_s / p_a}\right)^{(\gamma-1)/\gamma} - 1\right]} \tag{5}$$

3.2 Mixing Enhancement versus Shock Strength

The growth rate $\delta' = d\delta/dx$ of each jet is given by the slope of the axial thickness distribution (see Figure 17) . It is used here as a metric of mixing. We assemble all the growth rate data for our experiments (NPR=1.2-1.8 and A_e/A_t=1.2-1.8) and plot them versus their corresponding shock Mach number M_s. The resulting correlation, plotted in Figure19, shows an overall increasing trend but with considerable scatter. We realize that this is not a clean correlation because, in addition to the shock effect, there are other factors that influence the growth rate, namely the effects of density ratio and compressibility. For a perfectly expanded jet exhausting into a quiescent medium, there are two factors affecting its growth rate: the ambient-to-jet density ratio, and the convective Mach number. With increasing NPR, the density ratio decreases and the convective Mach number increases. Both trends have a suppressing effect on the growth rate. In the case of the severely-overexpanded CD nozzle, we have the additional destabilizing effect of the shock, whose strength increases with NPR.

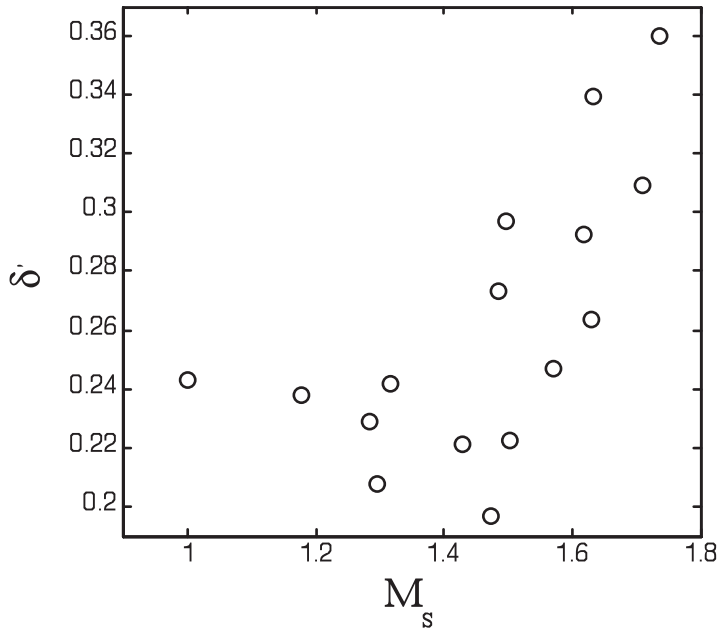

Figure 19. Correlation between growth rate and shock Mach number.

The effects of compressibility and density ratio can be filtered out by normalizing the growth rate by the perfectly expanded growth rate ($\delta'_{pe}=\delta'$ at A_e/A_t=1.0) for a given nozzle pressure ratio. The normalization invokes the single-stream shear layer growth rate relation (see for example Ref. 39)

$$\delta'_{pe} = C\left(1+\sqrt{\rho_a/\rho_e}\right)\left[0.23+0.77\exp\left(-3.5M_c^2\right)\right] \tag{6}$$

with the convective Mach number M_c defined as

$$M_c = \frac{U_e}{a_e + a_a} \tag{7}$$

The expression in the square brackets of Eq.6 describes the suppression of growth due to increased compressibility. The semi-empirical growth rate prediction of Eq. 6 is plotted versus NPR in Figure 20, along with the experimentally measured perfectly expanded growth rate, $\delta'_{pe} = \delta'$ at $A_e/A_t=1.0$. The excellent agreement between experiment and prediction verifies that there is suppression of jet mixing with increasing NPR due to compressibility and density effects. Normalizing the measured growth rate by the perfectly expanded value effectively removes these effects and isolates the mixing effects introduced by the internal shock wave. The normalized growth rate δ'/δ'_{pe} is plotted versus shock Mach number in Figure 21. There is a reasonable collapse of the data points, revealing the influence of the unsteady shock wave on jet mixing. The correlation shows that for shock Mach numbers less than 1.2, the jet remains unaffected by the presence of an internal shock wave, resulting from the lack of large-scale shock motion. Above this value, mixing enhancement increases very rapidly, with the growth rate doubling at M_s=1.7.

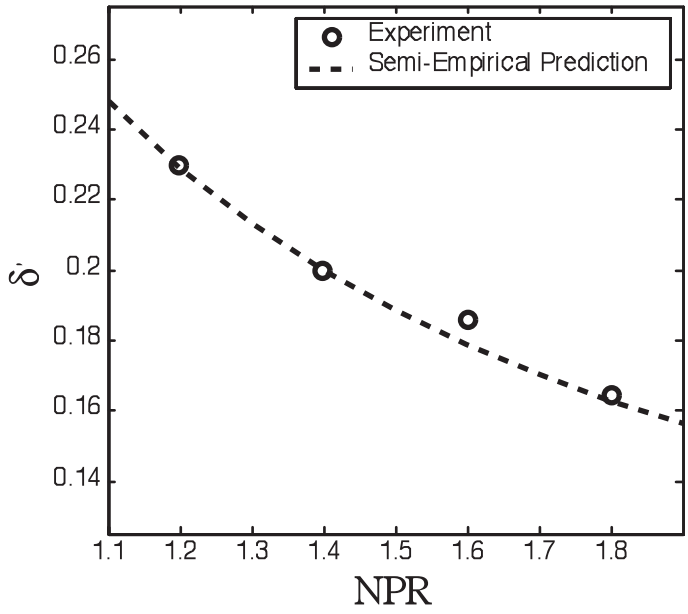

Figure 20. Nominal (perfectly expanded) growth rate versus nozzle pressure ratio

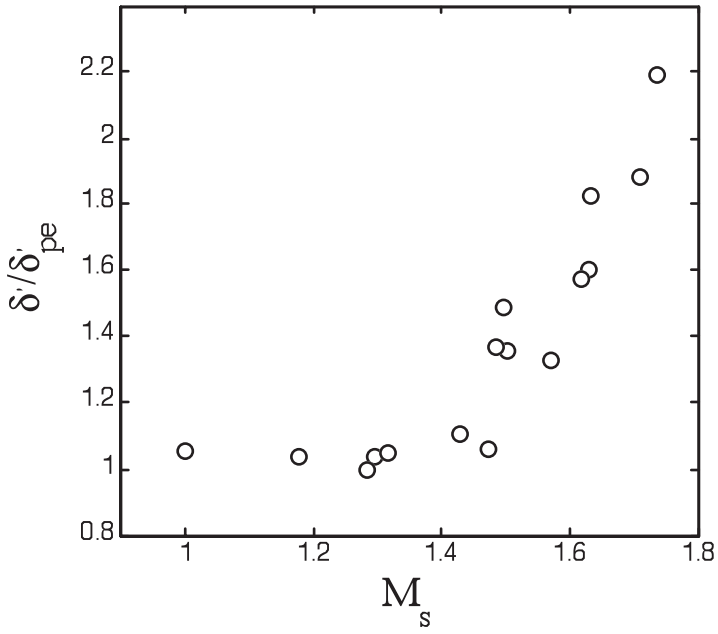

Figure 21. Correlation between normalized growth rate and shock Mach number.

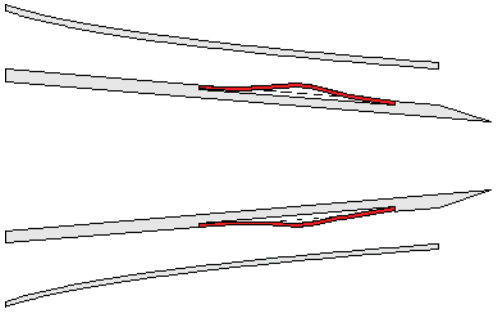

Figure 22 Variable geometry throat for on-demand application of mixing enhancement. Actuation could be pneumatic or mechanical.

4. CONCLUSIONS

Experiments have demonstrated the occurrence of instability in the plume of convergent-divergent nozzles operated at off-design conditions. This instability can enhance mixing in the flow itself or can be used to destabilize an adjacent flow. The latter feature enables mixing enhancement of an arbitrary jet via parallel injection of a secondary gas flow. The advantages of this method are that it involves a simple flow path and avoids complex mechanical mixing devices that generally lead to weight and maintenance penalties.

The results of preliminary experiments on axisymmetric nozzles suggest that mixing enhancement coincides with the occurrence of shock-induced separation inside the convergent-divergent nozzle. Accordingly, a fundamental investigation of supersonic nozzle flow separation was conducted in a planar nozzle facility. This study showed that the internal shock wave oscillates in a non-periodic, low-frequency motion with strong low-frequency content. The shock motion acts as a forcing input at the origin of the separation shear layer. The intensity of low-frequency shock oscillation increases with shock Mach number, and consequently the separation shear layer become more unstable. Mean velocity surveys of the plume of the planar nozzle revealed that, when properly normalized, the growth rate of the jet correlates well with the strength of the internal shock wave. For weak shocks (M_s<1.2), characterized by relatively small-scale motion, there is little effect on mixing in the nozzle plume. For stronger shocks, where large-scale motion is more prevalent, there is a sharp rise in the growth rate with increasing shock strength. Thus, the mixing enhancement phenomenon results from the excitation of the downstream flow by the unsteady internal shock wave.

The results imply a tradeoff between mixing enhancement and thrust loss in the nozzle (stronger shocks generate a larger total pressure loss). For applications involving fuel injection thrust is not a primary concern. However, for applications pertaining to propulsion, thrust considerations must be addressed. In a turbofan engine, the bypass nozzle is the most likely implementation of this method. For the typical conditions of mixing enhancement studied in round nozzles (A_e/A_t=1.3, NPR=1.8), direct and indirect measurements of thrust loss of CD nozzles[3,33,36] suggest a thrust loss of around 5%. For low-bypass, military applications, the overall thrust loss would be on the order of 1% and thus may be tolerable for the entire mission of the aircraft. For high-bypass applications, the simplicity of the flow path offers an on-demand strategy wherein compliant walls are actuated to form a convergent-divergent nozzle geometry when mixing enhancement is desired and a nominal geometry otherwise. An illustration of this concept is shown in Figure 22. This on-demand application would confine thrust losses to periods where mixing enhancement is activated.

ACKNOWLEDGMENTS

We are grateful for the support by the National University of Singapore, Temasek Labs (Contract No. TL/AE/2004/0001, monitored by Dr. Her Mann Tsai).

REFERENCES

1. Papamoschou, D., “Mixing Enhancement Using Axial Flow,” AIAA Paper 2000-0093.
2. Zaman, K.B.M.Q. and Papamoschou D., “Study of mixing enhancement observed with a co-annular nozzle configuration,” AIAA Paper 2000-0094, 2000.

3. Papamoschou D., Zill, A. and Johnson A., "Supersonic flow separation in planar nozzles," *Shock Waves*, 2008, 19(3), 171-183.
4. Johnson, A.D. and Papamoschou D., "Instability of shock-induced nozzle flow separation," to appear in *Physics of Fluids*.
5. Xiao, Q., Tsai, H.M. and Papamoschou, D., "Numerical investigation of supersonic nozzle flow separation," 2007, *AIAA Journal*, 45(3), 532-541.
6. Xiao, Q., Tsai, H.M., Papamoschou, D. and Johnson, A., "Experimental and numerical study of jet mixing from a shock-containing nozzle," *Journal of Propulsion and Power*, 2009, 25(3), 688-696.
7. Chen, H.H. and Driscoll, J.F., "Nitric oxide levels of turbulent jet diffusion flames-effects of coaxial air and other mixing parameters," *23rd Symposium on Combustion*, 1990.
8. Fric, T.F., "Effects of fuel-air unmixedness on NOx emmissions," *Journal of Propulsion and Power*, 1993, 9(5), 708-713.
9. Schetz, J.A., Hewitt, P.W. and Situ, M., "Transverse jet breakup and atomization with rapid vaporization along the trajectory," *AIAA Journal*, 1985, 23(4), 254-261.
10. Hermanson, J.C., Papas, P. and Kay, I.W., "Structure and penetration of a supersonic fluid jet in supersonic flow," *Journal of Propulsion and Power*, 1994, 10(3), 387-393.
11. Tillman, T.G., Paterson, R.W. and Presz, W.M., "Supersonic Nozzle Mixer Ejector," *Journal of Propulsion and Power*, 1992, 8(2), 513-519.
12. Sato, H., Mori, M. and Nakamura, T., "Development of a dry ultra low NOx double swirler staged gas turbine combustor," *Journal of Engineering for Gas Turbine and Power*, 1998, 120(1), 41-47.
13. Harari, R. and Sher, E., "Optimization of a plain-jet airblast atomizer," *Atomization and Sprays*, 1997, 7(1), 97-113.
14. Westley, R. and Lilley, G.M., "An investigation of the noise field from a small jet and methods for its reduction," College of Aeronautics, Report 53, Cranfield Univ., England, UK, 1952.
15. Seiner, J.M. and Gilinski, M.M., "Nozzle thrust optimization while reducing jet noise," *AIAA Journal*, 1997, 35(3), 420-427.
16. Ahuja, K.K. and Brown, W.H., "Shear flow control by mechanical tabs," AIAA-89-0994, 1989.
17. Zaman, K.B.M.Q., Reeder, M.F. and Samimy, M., "Control of an axisymmetric jet using vortex generators," *Physics of Fluids*, 1994, 6(2), 778-796.
18. Samimy, M., Kim, J.H., Clancy, P.S. and Martens, S., "Passive control of supersonic rectangular jets via nozzle trailing-edge modification," *AIAA Journal*, 1998, 36(7), 1230-1239.
19. Seiner, J.M. and Grosch, C.E., "Mixing enhancement by tabs in round supersonic jets," AIAA-98-2326, 1998.
20. Zaman, K.B.M.Q., "Spreading characteristics of compressible jets from nozzles of various geometries," *Journal of Fluid Mechanics*, 1999, 383, 197-228.
21. Samimy, M., Zaman, K.B.M.Q. and Reeder, M.F., "Effect of tabs on the flow and noise control of an axisymmetric jet," *AIAA Journal*, 1993, 31, 609-619.
22. Yu, K.H. and Schadow, K.C., "Cavity-actuated supersonic mixing and combustion control," *Combustion and Flame*, 1994, 99, 295-301.
23. Kumar, A., Bushnell, D.M. and Hussaini, M.Y., "Mixing augmentation technique for hypervelocity scramjets," *Journal of Propulsion and Power*, 1989, 5(5), 514-521.
24. Dolling, D.S., Fournier, E. and Shau, Y.R., "Effect of vortex generators on the growth of a compressible shear layer," *Journal of Propulsion and Power*, 1992, 8(5), 1049-1056.
25. Island, T.C., Urban, W.D. and Mungal, M., "Mixing enhancement in compressible shear layers via sub-boundary layer disturbances," *Physics of Fluids*, 1998, 10(4), 1008-1020.
26. Strykowksi, P.J., Krothapalli, A. and Jendoubi, S., "The effect of counterflow on the development of compressible shear layers," *Journal of Fluid Mechanics*, 1996, 308, 63-96.
27. Van der Veer, M.R. and Strykowski, P.J., "Counterflow thrust vector control of subsonic jets: continuous and bistable regimes," *Journal of Propulsion and Power*, 1997, 13(3), 412-420.
28. Raman, G., "Using controlled unsteady fluid mass addition to enhance jet mixing," *AIAA Journal*, 1997, 35(4), 647-656.

29. Weber, Y.S. and Bowers, D.L., "Advancements in exhaust system technology for the 21st century," AIAA-98-3100, 1998.
30. Smith, B.L. and Glezer, A., "Vectoring and small-scale motions effected in free shear flows using synthetic actuators," AIAA-99-0164, 1999.
31. Li, H. and Ben-Dor, G., "Mach reflection wave configuration in two-dimensional supersonic jets of overexpanded nozzles," *AIAA Journal*, 1996, 36(3), 488-491.
32. Romine, G.L., "Nozzle flow separation," *AIAA Journal*, 1998, 36(9), 1618-1625.
33. Wilmoth, R.G. and Leavitt, L.D., "Navier stokes predictions of multi-function nozzle flows," *Society of Automotive Engineers Transactions*, 1987, 96(6), 6.865-6.879.
34. Hamed, A. and Vogiatzis, C., "Overexpanded two-dimensional convergent-divergent nozzle flow simulations, assessment of turbulence models," *Journal of Propulsion and Power*, 1997, 13(3), 444-445.
35. Hamed, A. and Vogiatzis, C., "Overexpanded two-dimensional convergent-divergent nozzle flow performance, effects of three-dimensional flow interactions," *Journal of Propulsion and Power*, 1998, 14(2), 234-240.
36. Hunter, C.A., "Experimental, theoretical and computational investigation of separated nozzle flows," AIAA-98-3107, 1998.
37. Morrisette, E.L., and Goldberg, T.J., "Turbulent Flow Separation Criteria for Overexpanded Supersonic Nozzles," NASA TP 1207, 1978.
38. Reshotko, E., and Tucker, M., "Effect of a Discontinuity on Turbulent Boundary Layer Thickness Parameters with Application to Shock-Induced Separation," NACA TN-3454, 1955.
39. Murakami, E. and Papamoschou, D. "Mean Flow Development in Dual-Stream Compressible Jets," *AIAA Journal*, 2002, 40(6), 1131-1138.